Available online at www.sciencedirect.com
ScienceDirect
Trans. Nonferrous Met. Soc. China 28(2018) 1947−1957
Transactions of Nonferrous Metals Society of China
www.tnmsc.cn

Effect of hot deformation on $\alpha \rightarrow \beta$ phase transformation in 47Zr−45Ti−5Al−3V alloy

Yuan-biao TAN[1,2], Li-yuan Ji[2], Wen-chang LIU[2], Song XIANG[1], Fei ZHAO[1], Yi-long LIANG[1]

1. Guizhou Key Laboratory of Materials Structure and Strength, College of Materials and Metallurgy, Guizhou University, Guiyang 550025, China;
2. State Key Laboratory of Metastable Materials Science and Technology, College of Materials Science and Engineering, Yanshan University, Qinhuangdao 066004, China

Received 6 July 2017; accepted 10 November 2017

Abstract: The effect of strain rate and deformation temperature on the $\alpha \rightarrow \beta$ phase transformation in 47Zr−45Ti−5Al−3V alloy with an initial widmanstatten α structure was investigated. At the deformation temperature of 550 °C, the volume fraction of α phase decreased with increasing strain rate. At 600 and 650 °C, the volume fraction of α phase firstly increased to a maximum value with increasing strain rate from 1×10^{-3} to 1×10^{-2} s^{-1}, and then decreased. At 700 °C, the microstructure consisted of single β phase. At a given strain rate, the volume fraction of α phase decreased with increasing deformation temperature. With decreasing strain rate and increasing deformation temperature, the volume fraction and size of globular α phase increased. At 650 °C and 1×10^{-3} s^{-1}, the lamellar α phase was fully globularized. The variation in the volume fraction and morphology of α phase with strain rate and deformation temperature significantly affected the hardness of 47Zr−45Ti−5Al−3V alloy.
Key words: 47Zr−45Ti−5Al−3V alloy; hot deformation; phase transformation; Vickers hardness; microstructure

1 Introduction

Zirconium and its alloys have been employed in nuclear and chemical engineering applications for many years owing to their attractive comprehensive properties like low thermal neutron absorption cross section, admirable corrosion resistance, superior compatibility with the fuel and coolant, long-term dimensional stability in an irradiation environment and low cycle fatigue properties [1−4]. Nevertheless, the relatively low ultimate tensile strength of these Zr alloys limits their application fields [5,6]. A series of new ZrTiAlV alloys with ultra-high strength and good ductility have been recently designed as advanced structural materials in the aerospace field [7−9]. 47Zr−45Ti−5Al−3V alloy is one of the most typical ZrTiAlV alloys. It is well known that the mechanical properties of metallic alloys are very sensitive to the characteristics of microstructure, such as phase component and morphology. Thus, it is important to study the effect of heat treatment and hot deformation on the phase transformation and microstructure of the ZrTiAlV alloys.

A large number of investigations have been carried out to study the effect of heat treatment on the phase transformation of Ti or Zr alloys in recent years [10−15]. JING et al [11] found that the thickness of α phase precipitated from the β phase was sensitive to the annealing temperature in the 71Ti−19Zr−7Al−3V alloy. With increasing annealing temperature, the α phase tended to exhibit equiaxed grains, except for the specimen annealed at 1050 °C. The tensile strength of the alloy increased with an increase in the number of equiaxed α grains. QU et al [14] reported that the volume fraction of β phase in the furnace cooling specimens increased from about 5.7% to 36.2%, and then slightly decreases to 30.2% with increasing annealing temperature from 500 to 800 °C in the β-51Zr−40Ti−5Al−4V alloy.

Hot deformation parameters, such as deformation temperature, strain rate and strain, significantly affected the final microstructure of Ti or Zr alloys during the hot

Foundation item: Project (201629) supported by the Scientific Research Foundation for Introduced Talent of Guizhou University, China; Projects (20164014, 20165654) supported by the Hundred-level Innovative Talents Project of Guizhou Province, China; Project (20146013) supported by the Science and Technology of Guizhou Province, China
Corresponding author: Yuan-biao TAN; Tel: +86-14785158006; E-mail: ybtan1@gzu.edu.cn
DOI: 10.1016/S1003-6326(18)64840-X

deformation [16−23]. SESHACHARYULU and DUTTA [18] found that the lamellar α grains formed in low strain rate ($\leq 1\times10^{-1}$ s^{-1}) experiments were coarser as compared to the equiaxed α grains formed in high strain rate (1−100 s^{-1}) experiments in Ti−6Al−4V alloy. YU et al [19] investigated the effect of deformation parameters on the precipitation mechanism of secondary α phase under high temperature isothermal compression of Ti−6Al−4V alloy. The morphology of the secondary α phase transformed gradually from lamellar colony to equiaxed morphology with increasing strain rate or decreasing deformation temperature. The globularization kinetics of α phase in Ti−6Al−2Sn−4Zr−6Mo alloy was affected by deformation [20]. The volume fraction of globular α phase gradually increased from zero in un-deformed sample to about 10% in a sample deformed to a strain of 1.0. FAN et al [21] also reported that pre-deformation and low speed deformation accelerated the dynamic globularization of α strips during hot deformation. TAN et al [23] studied the hot deformation behavior of 47Zr−45Ti−5Al−3V alloy with a coarse grain structure in the β phase field. They found that dynamic recovery occurred at low temperatures and high strain rates, whereas very coarse recrystallized grains were obtained at high temperatures and low strain rates.

The hot deformation behavior of Ti or Zr alloys is also affected by the initial microstructure. LUO et al [24] reported the deformation behavior of Ti−5Al−2Sn−2Zr−4Mo−4Cr alloy with two initial microstructures during hot working. The results showed that the initial microstructures had a significant effect on the dynamic globularization of α phase. The dynamic globularization of α phase occurring in the alloy with widmanstatten α plates was easier than that in the alloy with equiaxed and elongated α phase. SESHACHARYULU et al [25,26] studied the hot working of Ti−6Al−4V with an equiaxed $\alpha+\beta$ microstructure or lamellar starting structure. They found that the flow stress of Ti−6Al−4V alloy with a lamellar structure was higher than that with an equiaxed $\alpha+\beta$ microstructure, and the grain size of α phase after hot deformation in the former was thinner than that in the latter. TAN et al [27] studied the hot deformation behavior of 47Zr−45Ti−5Al−3V alloy with an initial widmanstatten α structure. It was found that the initial widmanstatten α structure had a significant effect on the grain refinement of β phase in the 47Zr−45Ti−5Al−3V alloy after hot deformation. It is obvious that the grain refinement of β phase is related to the $\alpha\rightarrow\beta$ phase transformation occurring during hot deformation. In the present work, hot compression tests were conducted on the 47Zr−45Ti−5Al−3V alloy with an initial widmanstatten α structure at deformation temperatures from 550 to 700 °C and strain rates from 1×10^{-3} to 1×10^{0} s^{-1}, and the effect of hot deformation parameters on the $\alpha\rightarrow\beta$ phase transformation was investigated.

2 Experimental

Sponge Zr (w(Zr)+w(Hf) ≥99.5%), sponge Ti (99.7%), industrially pure Al (99.5%), and V (99.9%) were used to prepare the 47Zr−45Ti−5Al−3V (mass fraction, %) alloy. The detailed preparation procedure was described in the previous paper [28]. The phase transformation temperature of the 47Zr−45Ti−5Al−3V alloy was measured at a heating rate of 5 °C/min by differential scanning calorimetry. The transformation temperatures of $\alpha\rightarrow\alpha+\beta$ and $\alpha+\beta\rightarrow\beta$ in this alloy were obtained to be 600 and 703 °C, respectively [27]. In order to investigate the effect of hot deformation parameters on the transformation of $\alpha\rightarrow\beta$ phase, the alloy was annealed at 850 °C for 30 min in a tubular vacuum heat-treatment furnace with a protective argon atmosphere followed by furnace cooling to obtain a microstructure with α phase. The microstructure and XRD pattern of the 47Zr−45Ti−5Al−3V alloy annealed at 850 °C for 30 min are shown in Fig. 1. It was observed that the microstructure consisted of a large amount of lamellar α phases distributed in the β matrix. The volume fraction of α phase was calculated from Fig. 1(b) to be about 96.1%.

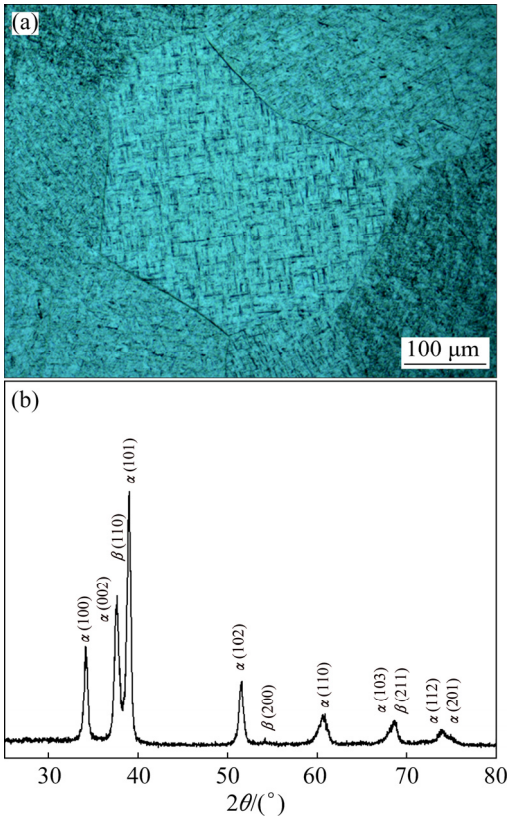

Fig. 1 Microstructure (a) and XRD pattern (b) of 47Zr−45Ti−5Al−3V alloy heat-treated at 850 °C for 30 min followed by furnace cooling

Cylindrical compression specimens with 12 mm in height and 8 mm in diameter were cut from the heat-treated bars. Hot compression tests were performed on a Gleeble 3500 thermo-mechanical simulator in the deformation temperature range of 550−700 °C with 50 °C interval and strain rate range of 1×10^{-3}−1×10^{0} s^{-1}. The specimens were heated by the direct resistance heating system. The temperature was controlled with a thermo-couple spot welded at the mid-span of the specimen. The graphite lubricant was coated on the top and bottom surfaces of specimen, and the tantalum chip of 0.1 mm in thickness was placed on the both ends of the cylindrical specimen to assist in reducing friction. Hot compression tests were carried out in an argon atmosphere. Specimens were heated to deformation temperature at a rate of 20 °C/s and then held for 10 min. The specimens were deformed to a true strain of 0.7 at deformation temperatures of 550−700 °C and strain rates of 1×10^{-3}−1×10^{0} s^{-1}. Immediately, after deformation, the specimens were rapidly quenched with water sprays for the purpose of preserving the deformed microstructures. In order to examine the microstructure before hot deformation, the 47Zr−45Ti−5Al−3V alloy was annealed at different deformation temperatures for 10 min followed by quenching with water sprays.

Vickers hardness tests were performed on an FM-ARS 9000 hardness tester for deformed specimens. A load of 5 N was applied for 10 s at each location. The deformed specimens were sectioned parallel to the compression axis along the center of specimen. Specimens were mechanically polished and chemically etched by the solution with 10% HF + 45% HNO_3 + 45% H_2O (volume fraction). The microstructures before and after hot deformation were examined using the Axiovert 200 MAT optical microscopy (OM) and HITACHI S−4800 scanning electron microscopy (SEM). The phase component of specimens was determined by D/MAX−2500/PC X-ray diffractometer (XRD) with Cu K_α radiation and a graphite monochromator operated at 40 kV and 200 mA.

Considering the fact that there are only two phases in the 47Zr−45Ti−5Al−3V alloy after hot deformation, the volume fraction of α phase (f_α) in the alloy can be calculated using the direct comparison method by XRD [29]:

$$f_\alpha = \frac{1}{1+\dfrac{1}{m}\sum_{i=1}^{m}\left(\dfrac{I_i^\beta}{R_i^\beta}\right)\Big/\dfrac{1}{n}\sum_{i=1}^{n}\left(\dfrac{I_i^\alpha}{R_i^\alpha}\right)} \tag{1}$$

where m and n represent the numbers of diffraction peaks of β and α phases used in calculation, respectively, I is the integrated intensity for a diffraction peak corresponding to β or α phase, and R_i is the material scattering factor and given by the following equation:

$$R_i = \frac{1}{V^2}\left[|F_i|^2 P_i\left(\frac{1+\cos^2 2\theta}{\sin^2\theta\cos\theta}\right)\right]e^{-2M} \tag{2}$$

where V is the volume of the unit cell, F_i is the structure factor, P_i is the multiplicity factor, θ is the angle, and e^{-2M} is the temperature factor. In this study, the (110) and (200) diffraction peaks of β phase as well as the $(10\bar{1}0)$, (0002), $(10\bar{1}1)$, $(10\bar{1}2)$ and $(11\bar{2}0)$ diffraction peaks of α phase were used to calculate the volume fractions of the β and α phases. In this case, the effect of texture on the volume fraction of the β phase can be weakened. Table 1 lists the volume fractions of α phase in the 47Zr−45Ti−5Al−3V alloy under different hot deformation conditions.

Table 1 Volume fractions of α phase in 47Zr−45Ti−5Al−3V alloy deformed at different temperatures and strain rates

$\dot{\varepsilon}$ /s^{-1}	Volume fraction/%			
	550 °C	600 °C	650 °C	700 °C
Holding for 10 min	79.7	70.1	55.6	0
1×10^{-3}	78.2	41.0	24.2	0
1×10^{-2}	73.5	49.4	35.1	0
1×10^{-1}	59.7	47.9	31.6	0
1×10^{0}	50.5	38.4	30.4	0

3 Results

3.1 Phase component and microstructure of specimen before hot deformation

In order to fully evaluate the influence of hot deformation parameters on the phase transformation occurring in the 47Zr−45Ti−5Al−3V alloy, it is pertinent to have a detailed knowledge of the phase component and microstructure that exist immediately before deformation. Figure 2 shows the XRD patterns of the 47Zr−45Ti−5Al−3V alloy annealed at annealing temperatures from 550 to 700 °C for 10 min followed by quenching with water spray before hot deformation. The phase component of the alloy was significantly influenced by annealing temperature. At 550 °C, more α phase diffraction peaks existed and the intensity of the diffraction peaks of α phase was higher than that of β phase, indicating that the alloy consisted of a large number of α phases and a small number of β phases. With increasing annealing temperature from 550 to 650 °C, the $(10\bar{1}1)$ diffraction peak of α phase at 2θ about 39° gradually narrowed and the intensity of the diffraction peak decreased. When the annealing temperature increased to 700 °C, only the diffraction peaks of β phase were observed in the XRD pattern. Figure 3 shows the variation in the volume fraction of α phase with annealing temperature in the 47Zr−45Ti−

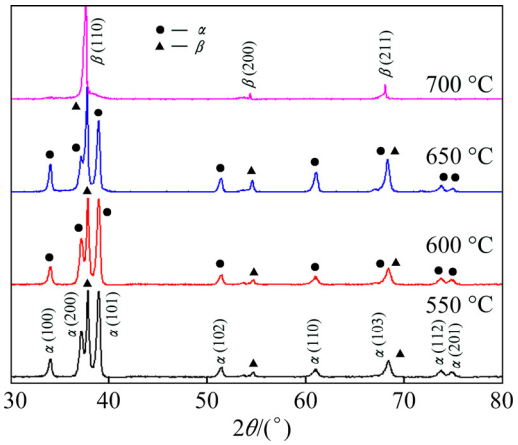

Fig. 2 XRD patterns of 47Zr−45Ti−5Al−3V alloy with initial widmanstatten α structure at different annealing temperatures before deformation

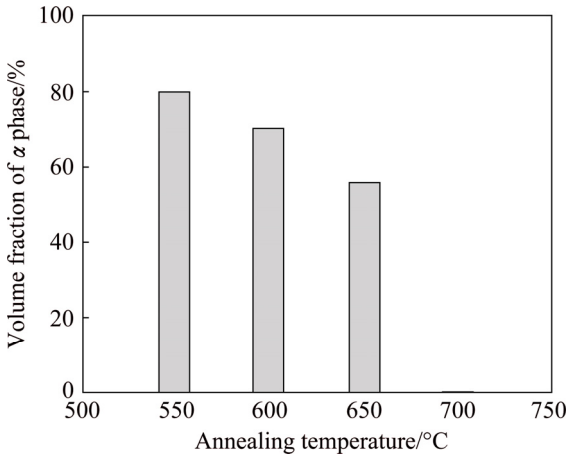

Fig. 3 Variation in volume fraction of α phase with annealing temperature before deformation in 47Zr−45Ti−5Al−3V alloy with initial widmanstatten α structure

5Al−3V alloy with an initial widmanstatten α structure. The volume fraction of α phase was about 79.7% at the deformation temperature of 550 °C. With increasing annealing temperature to 650 °C, the volume fraction of α phase decreased to 55.6%. When the annealing temperature was raised to 700 °C, the microstructure was completely composed of single β phase.

Figure 4 shows the optical microstructures of the 47Zr−45Ti−5Al−3V alloy annealed at different annealing temperatures from 550 to 700 °C for 10 min. It was seen that a large amount of lamellar α phases were observed in the interior of equiaxed β grains at 550 °C (Fig. 4(a)). With increasing annealing temperature, the volume fraction of α phase decreased significantly, whereas the volume fraction of β phase increased (Figs. 4(b) and (c)). When the annealing temperature was 700 °C, the α phase was fully transformed into the β phase, and the microstructure consisted of single β phase (Fig. 4(d)).

3.2 Phase component and microstructure of specimen after hot deformation

Figure 5 shows XRD patterns of the 47Zr−45Ti−

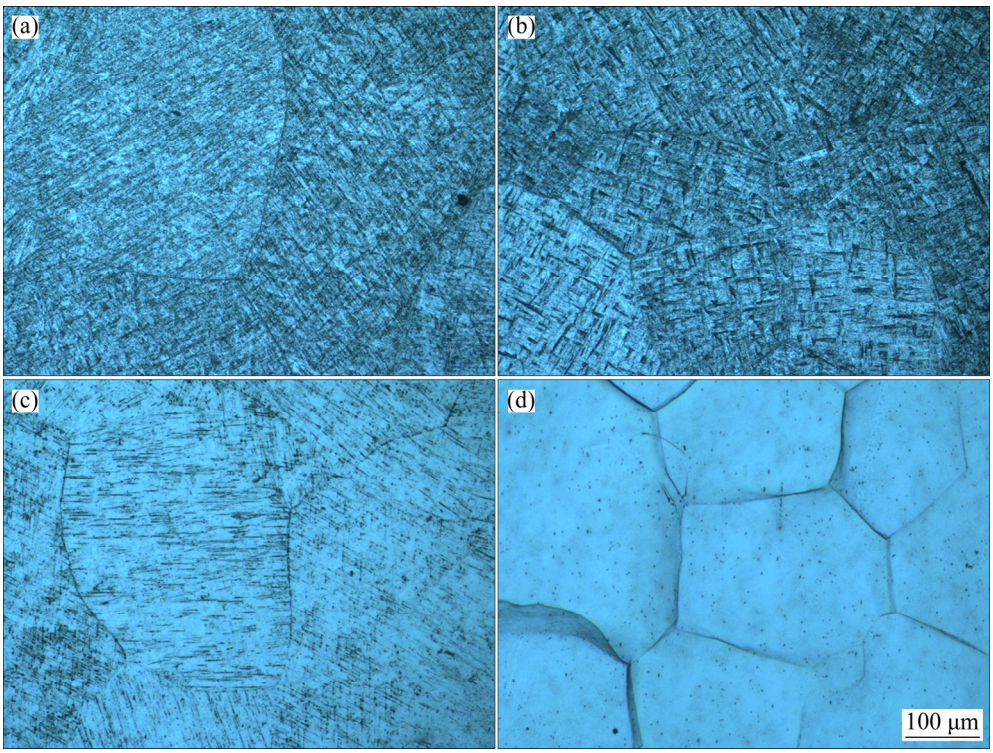

Fig. 4 Optical microstructures of 47Zr−45Ti−5Al−3V alloy with initial widmanstatten α structure annealed at 550 °C (a), 600 °C (b), 650 °C (c) and 700 °C (d) respectively for 10 min

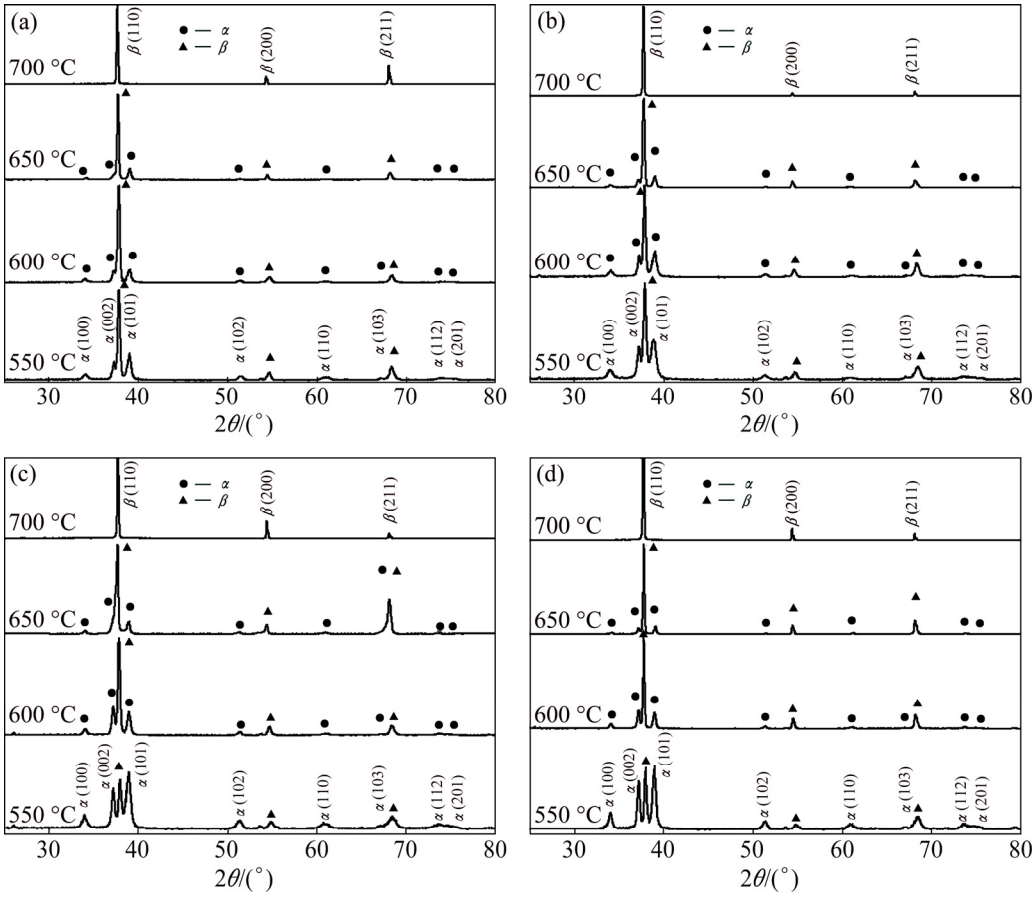

Fig. 5 XRD patterns of 47Zr−45Ti−5Al−3V alloy deformed at strain rates of 1×10^{0} s^{-1} (a), 1×10^{-1} s^{-1} (b), 1×10^{-2} s^{-1} (c) and 1×10^{-3} s^{-1} (d)

5Al−3V alloy deformed at deformation temperatures from 550 to 700 °C and strain rates from 1×10^{-3} to 1×10^{0} s^{-1}. It was seen that the intensities of the diffraction peaks of α and β phases varied with deformation temperature and strain rate. Figure 6 shows the variation in the volume fraction of α phase with strain rate at different deformation temperatures after hot deformation. At the deformation temperature of 550 °C, the volume fraction of α phase decreased from 78.2% to 50.5% with increasing strain rate from 1×10^{-3} to 1×10^{0} s^{-1}. At 600 and 650 °C, the volume fraction of α phase firstly increased to a maximum value with increasing strain rate from 1×10^{-3} to 1×10^{-2} s^{-1}, and then decreased. Compared with the volume fraction of α phase before hot deformation, the volume fraction of α phase after hot deformation was lower, indicating that the hot deformation promoted the $\alpha\rightarrow\beta$ phase transformation. At a given strain rate the volume fraction of α phase decreased with increasing deformation temperature.

Figure 7 shows the SEM microstructures of the 47Zr−45Ti−5Al−3V alloy deformed under different conditions in the $\alpha+\beta$ phase field. At the deformation temperature of 550 °C and the strain rate of 1×10^{0} s^{-1},

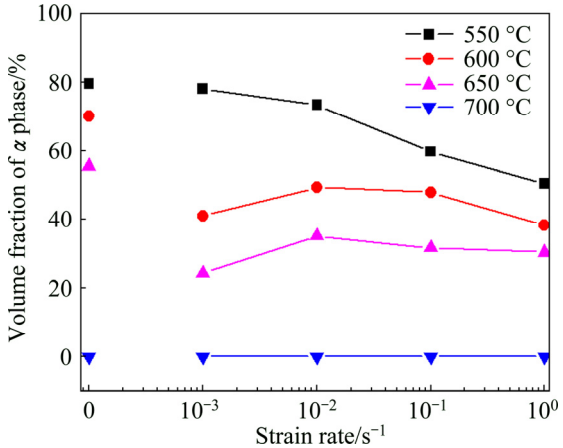

Fig. 6 Variation in volume fraction of α phase with strain rate at different deformation temperatures (For comparison, the volume fraction of α phase before deformation is given in this figure)

a large amount of lamellar α phases were observed (Fig. 7(a)). To clearly observe the deformed microstructure of the alloy, a detailed characterization of microstructure via TEM is shown in Figs. 8(a) and (b). A small amount of globular α phases were observed in addition to the lamellar α phases, indicating that the

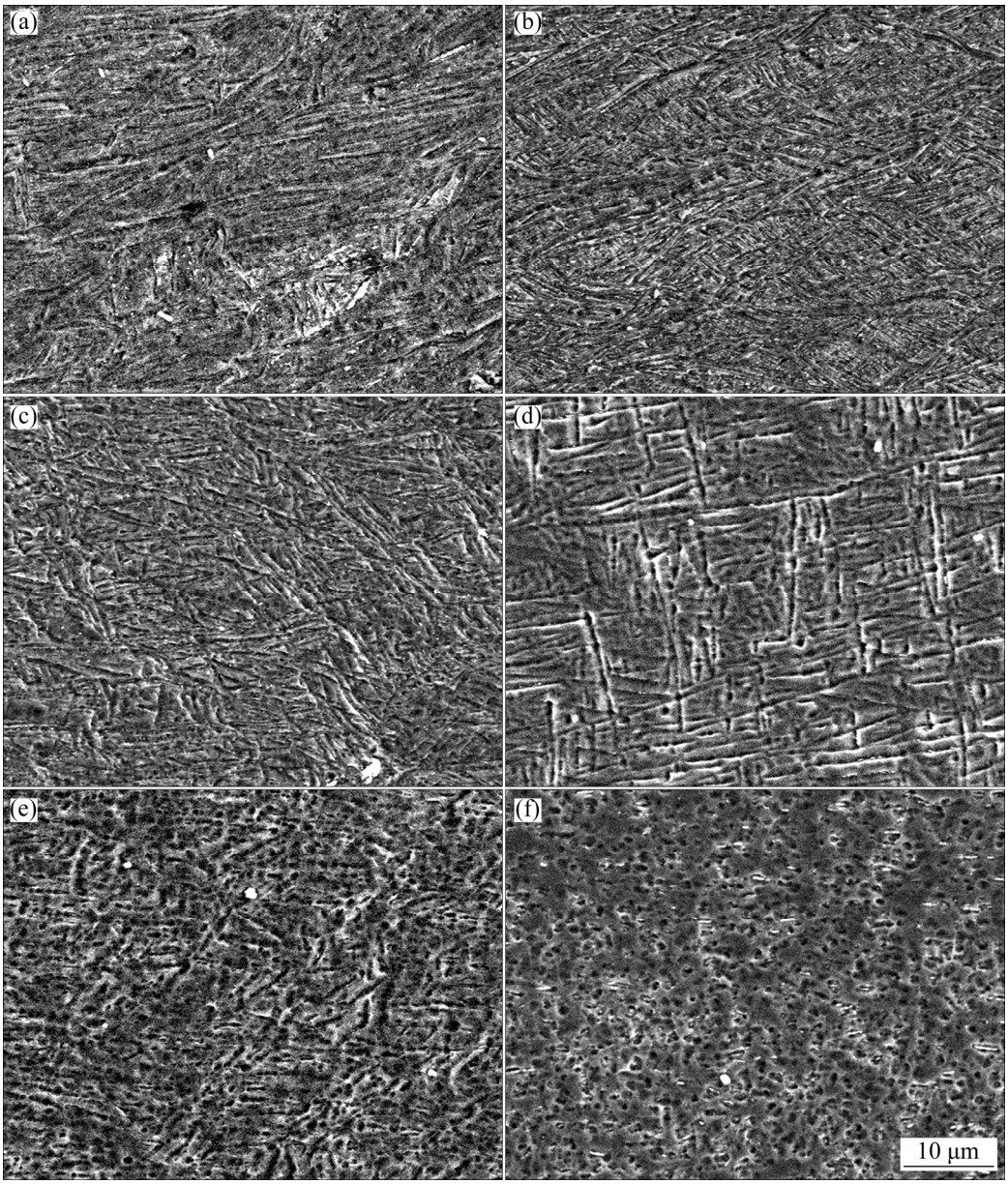

Fig. 7 SEM microstructures of 47Zr−45Ti−5Al−3V alloy with initial widmanstatten α structure deformed in α+β phase field under different conditions: (a) 550 °C, 1×10^{0} s^{-1}; (b) 550 °C, 1×10^{-2} s^{-1}; (c) 550 °C, 1×10^{-3} s^{-1}; (d) 600 °C, 1×10^{-2} s^{-1}; (e) 650 °C, 1×10^{-2} s^{-1}; (f) 650 °C, 1×10^{-3} s^{-1}

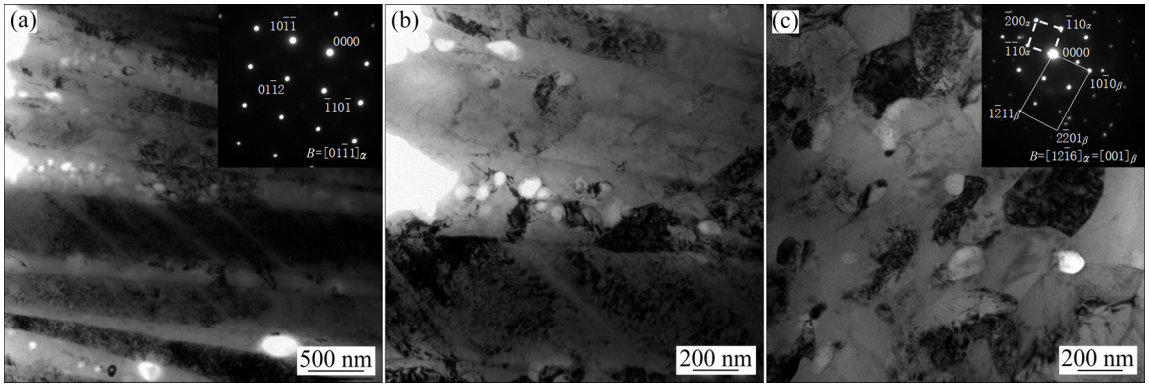

Fig. 8 TEM bright-field images of 47Zr−45Ti−5Al−3V alloy deformed at 550 °C, 1×10^{0} s^{-1} (a, b) and 600 °C, 1×10^{-2} s^{-1} (c)

globularization process occurred during hot deformation. The size of globular α phase was about 50 nm in diameter. With decreasing strain rate and increasing deformation temperature, the volume fraction and size of globular α phase increased (Figs. 7(b) to (e) and Fig. 8(c)). When the deformation temperature was 650 °C and the strain rate was 1×10^{-3} s^{-1}, the lamellar α phase was fully globularized (Fig. 7(f)). This indicated that the higher deformation temperature and lower strain rate accelerated the dynamic globularization of initial widmanstatten α phase. Similar results were also observed in TA15 titanium alloy with primary strip α structure [21] and Ti−6.5Al−2Zr−1Mo−1V alloy with lamellar microstructure [30]. This is because dynamic globularization is a thermal activation process. At higher temperatures or lower strain rates, the diffusion rate is fast and the diffusion time is sufficient.

Figure 9 shows the optical microstructures of the 47Zr−45Ti−5Al−3V alloy deformed at 700 °C and different strain rates. It was seen that the coarse β grains were elongated perpendicularly to the compression axis with some serrated grain boundaries at the strain rate of 1×10^{0} and 1×10^{-1} s^{-1} (Figs. 9(a) and (b)), respectively, indicating that only dynamic recovery occurred during hot deformation. At the strain rate of 1×10^{-2} s^{-1} (Fig. 9(c)), a few fine recrystallized grains appeared at the initial grain boundaries of deformed grains. The volume fraction and grain size of recrystallized grains increased with decreasing strain rate (Fig. 9(d)).

3.3 Vickers hardness

Figure 10 shows the variation in Vickers hardness with strain rate at different deformation temperatures in the 47Zr−45Ti−5Al−3V alloy with an initial widmanstatten α structure. At the deformation temperature of 550 °C, Vickers hardness firstly increased to a maximum value of HV 430 with increasing strain rate from 1×10^{-3} to 1×10^{-2} s^{-1}, and then decreased to HV 411 at the strain rate of 1×10^{0} s^{-1}. At 600 and 650 °C, the variation in Vickers hardness with strain rate also showed a similar trend. Vickers hardness firstly increased to a maximum value with increasing strain rate from 1×10^{-3} to 1×10^{-1} s^{-1}, and then decreased with further increasing strain rate to 1×10^{0} s^{-1}. When the deformation temperature was raised to 700 °C, Vickers hardness increased slightly with increasing strain rate. The deformation temperature strongly affected the Vickers hardness of 47Zr−45Ti− 5Al−3V alloy. Vickers hardness decreased significantly with increasing deformation temperature in the $\alpha+\beta$ field. The variation in Vickers hardness with temperature in the $\alpha+\beta$ phase field is consistent with the results obtained in 70.65Ti−19.2Zr−6.65Al−3.5V [11], β-51.1Zr−40.2Ti−4.5Al−4.2V [14] and 50Ti−30Zr−10Nb−10Ta alloys [31].

4 Discussion

4.1 Effect of strain rate and deformation temperature on $\alpha\rightarrow\beta$ phase transformation

A significant variation in phase component is

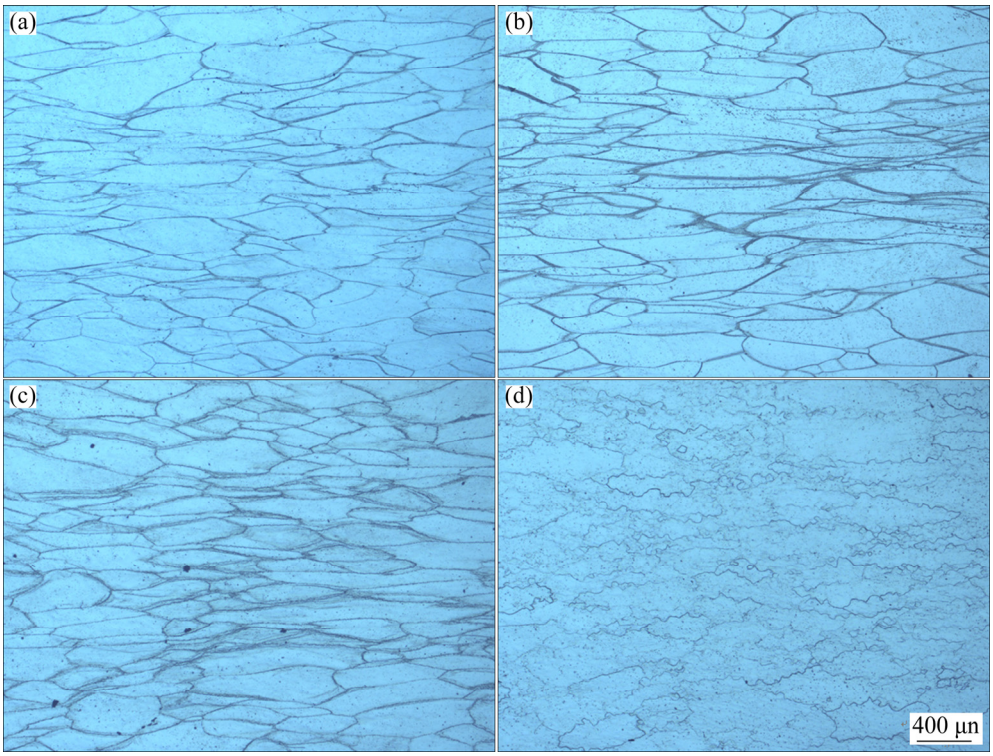

Fig. 9 Optical microstructures of 47Zr−45Ti−5Al−3V alloy deformed at 700 °C and strain rates of 1×10^{0} s^{-1} (a), 1×10^{-1} s^{-1} (b), 1×10^{-2} s^{-1} (c) and 1×10^{-3} s^{-1} (d)

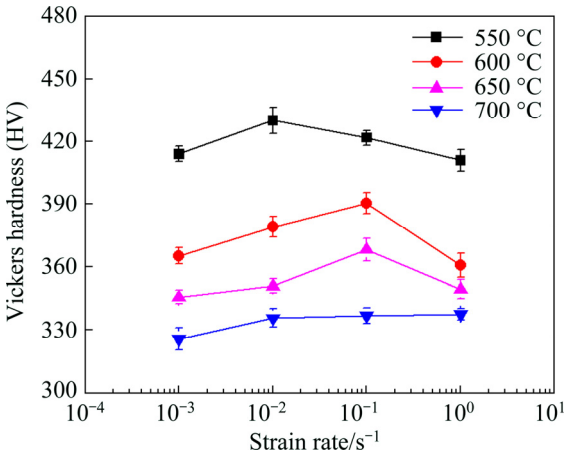

Fig. 10 Variation in Vickers hardness of 47Zr−45Ti−5Al−3V alloy with strain rate at different deformation temperatures after deformation

observed in the 47Zr−45Ti−5Al−3V alloy subjected to hot deformation at different strain rates and deformation temperatures. This is mainly attributed to the formation of defects and the atomic diffusion during hot deformation, which are effectively influenced by the strain rate [32]. For one reason, the defects such as dislocations and deformation bands sharply grow in number or quantity with increasing strain rate during hot deformation, which results in a continuous increase of deformation-stored energy. The dislocations accumulated during hot deformation provide the vantage locations for the β phase nucleation, and the deformation-stored energy accumulated during the hot deformation can provide the driving force for the $\alpha\rightarrow\beta$ phase transformation. Thus, the rate of $\alpha\rightarrow\beta$ phase transformation should increase with increasing strain rate. For another reason, when the specimens are deformed at a lower strain rate, the deformation time is longer at a given deformation temperature, which makes the diffusion of atoms easier and contributes to the growth of grain, and hence accelerates the process of the $\alpha\rightarrow\beta$ phase transformation. Thus, the rate of $\alpha\rightarrow\beta$ phase transformation should increase with decreasing strain rate. As the results of the two factors, the rate of $\alpha\rightarrow\beta$ phase transformation at higher and lower deformation temperatures follows different variation trends. When the deformation temperature was 600 or 650 °C, the atom diffusion rate is higher and the deformation time is longer with decreasing strain rate, which are beneficial to the $\alpha\rightarrow\beta$ phase transformation. With the increase of strain rate, the atom diffusion rate has a weakening effect on the $\alpha\rightarrow\beta$ phase transformation, which results in the defects and deformation-stored energy being the main factor. So, the rate of $\alpha\rightarrow\beta$ phase transformation firstly decreased and then increased with increasing strain rate. However, at the lowest deformation temperature of 550 °C, the driving force for the phase transformation is low and the diffusion of atoms is difficult, which are not conducive to the $\alpha\rightarrow\beta$ phase transformation. In this case, the main affecting factor is the accumulated dislocations which lead to the increase in the rate of $\alpha\rightarrow\beta$ phase transformation with increasing strain rate.

The rate of $\alpha\rightarrow\beta$ phase transformation varies evidently with deformation temperature, which can be attributed to the difference in the migration rate of atoms and the driving force for the phase transformation. Since the $\alpha\rightarrow\beta$ phase transformation belongs to diffusion phase transformation, which is mainly influenced by the atom diffusion rate and the driving force for phase transformation [11,33]. Generally, the frequency of the atom migration increases gradually with increasing temperature. In the insulation process, the moving distance of Al atom (which is α stabilized element) and V atom (which is β stabilized element) is different. During hot deformation, α phase is transformed into β phase which causes the V atom enriched, leading to the increase in the volume fraction of β phase. With increasing temperature, the difference in atom migration between Al and V becomes larger, which is beneficial to the transformation of $\alpha\rightarrow\beta$ phase. Moreover, according to the analysis by BURKE [34], grain growth takes place by atom diffusion across the grain boundary. The migration rate of grain boundary is proportional to $\exp[-Q_g/(RT)]$ according to the Arrhenius relationship. Thus, the growth rate of β phase grain increases with increasing temperature during hot deformation. On the other hand, the higher deformation temperature provides a larger driving force for the nucleation and growth of β phase, leading to the improvement of the $\alpha\rightarrow\beta$ phase transformation [35].

4.2 Effect of hot deformation on Vickers hardness

It is seen from Fig. 10 that the strain rate and deformation temperature have a significant effect on the Vickers hardness of 47Zr−45Ti−5Al−3V alloy. This can be attributed to the accumulated dislocations, the volume fraction of residual α phase and the morphology of α phase [12,31]. The dislocations that accumulated during hot deformation enhance Vickers hardness. Since the accumulated dislocations increase with increasing strain rate, the Vickers hardness of 47Zr−45Ti−5Al−3V alloy increases with increasing strain rate. The 47Zr−45Ti−5Al−3V alloy consists of α and β phases during hot deformation. The α phase has an HCP crystal structure with a higher value of Vickers hardness, while the β phase has a BCC crystal structure which has a weakening effect on the material. Thus, it is concluded that the Vickers hardness of 47Zr−45Ti−5Al−3V alloy depends

mainly on the volume fraction and morphology of α phase except for the accumulated dislocations. The variation in the volume fraction of α phase with strain rate and temperature is shown in Fig. 6. At the deformation temperature of 550 °C, the volume fraction of α phase decreases with increasing strain rate, leading to the decrease in Vickers hardness with strain rate. However, when the strain rate is 1×10^{-3} s^{-1}, the Vickers hardness of 47Zr−45Ti−5Al−3V alloy has a lower value, which is related to the thickness of α lath. The retention time at 550 °C is longer with decreasing strain rate, which makes the diffusion of atoms easier and contributes to the growth of grain. As a result, the thickness of α lath increases with decreasing strain rate. According to the Hall−Petch equation, Vickers hardness decreases with the increase of the thickness of α lath since increasing α lath thickness decreases the density of the phase boundary in the same cross-sectional area [11]. Therefore, the Vickers hardness of 47Zr−45Ti−5Al−3V alloy firstly increases with increasing strain rate and then decreases when the deformation temperature is 550 °C. At the deformation temperatures of 600 and 650 °C, the volume fraction of α phase firstly increases with decreasing strain rate from 1×10^{0} to 1×10^{-1} s^{-1}, leading to the increase in Vickers hardness with decreasing strain rate. At the strain rate of 1×10^{-2} s^{-1}, the Vickers hardness of 47Zr−45Ti−5Al−3V alloy decreased, which is effectively influenced by the morphology of α phase. The lamellar α phase is partially globularized when the strain rate is 1×10^{-2} s^{-1}. The lamellar microstructure is usually preferable for the strength, fracture toughness and fatigue crack propagation, while the globular microstructure is better for the ductility and fatigue crack initiation [36,37]. Thus, the Vickers hardness of 47Zr−45Ti−5Al−3V alloy has a lower value at a strain rate of 1×10^{-2} s^{-1}. With further decrease to 1×10^{-3} s^{-1}, Vickers hardness decreases owing to the decreasing volume fraction of α phase and the increasing volume fraction of globular α phase. At the deformation temperature of 700 °C, the microstructure consists of single β phase. The Vickers hardness of 47Zr−45Ti−5Al−3V alloy depends mainly on the degree of dynamic recrystallization. It is seen from Fig. 9 that the volume fraction and grain size of recrystallized grains increase with decreasing strain rate, which results in the decrease in Vickers hardness with decreasing strain rate.

5 Conclusions

1) At the deformation temperature of 550 °C, the volume fraction of α phase decreased from 78.2% to 50.5% with increasing strain rate from 1×10^{-3} to 1×10^{0} s^{-1}. At 600 and 650 °C, the volume fraction of α phase firstly increased with increasing strain rate from 1×10^{-3} to 1×10^{-2} s^{-1}, and then decreased. At a given strain rate, the volume fraction of α phase decreased with increasing deformation temperature. Hot deformation promoted the $\alpha\rightarrow\beta$ phase transformation.

2) A large amount of lamellar α phases were observed at the deformation temperature of 550 °C and strain rate of 1×10^{0} s^{-1}. With decreasing strain rate and increasing deformation temperature, the volume fraction and size of globular α phase increased. At the deformation temperature of 650 °C and strain rate of 1×10^{-3} s^{-1}, the lamellar α phase was fully globularized.

3) At the deformation temperature of 700 °C and strain rate of 1×10^{0} s^{-1}, the β grains were elongated perpendicularly to the compression axis with some serrated grain boundaries. With decreasing strain rate, the volume fraction of recrystallized grains increased.

4) At deformation temperatures of 550, 600 and 650 °C, Vickers hardness firstly increased to a maximum value with increasing strain rate and then decreased. At 700 °C, Vickers hardness increased slightly with increasing strain rate. At a given strain rate, Vickers hardness decreased significantly with increasing deformation temperature in the $\alpha+\beta$ phase field.

References

[1] FRANKLIN D G, LUCAS G E, BEMENT A L. Creep of zirconium alloys in nuclear reactors [S]. ASTM STP 815. Philadelphia, 1983.

[2] ZHANG X Y, SHI M H, LI C, LIU N F, WEI Y M. The influence of grain size on the corrosion resistance of nanocrystalline zirconium metal [J]. Materials Science and Engineering A, 2007, 448: 259−263.

[3] JUNG Y, SEOL Y N, CHOI B K, PARK J Y. Behavior of stress-relaxation and the estimation of creep in Zr−1.1Nb−0.05Cu alloy [J]. Materials and Design, 2012, 42: 118−123.

[4] ZHOU F Y, WANG B L, QIU K J, LIN W J, LI L, WANG Y B, NIE F L, ZHENG Y F. Microstructure, corrosion behavior and cytotoxicity of Zr−Nb alloys for biomedical application [J]. Materials Science and Engineering C, 2012, 32(4): 851−857.

[5] KISHORE R, SINGH R N, DEY G K, SINHA T K. Age hardening of cold-worked Zr−2.5wt%Nb pressure tube alloy [J]. Journal of Nuclear Materials, 1992, 187(1): 70−73.

[6] YANG Z N, LIU F C, ZHANG F C, YAN Z G, XIAO Y Y. Microstructural evolution and mechanical properties in Zr705 during the rolling process [J]. Materials Science and Engineering A, 2012, 544: 54−58.

[7] LIANG S X, MA M Z, JING R, ZHANG X Y, LIU R P. Microstructure and mechanical properties of hot-rolled ZrTiAlV alloys [J]. Materials Science and Engineering A, 2012, 532: 1−5.

[8] LIANG S X, MA M Z, JING R, ZHOU Y K, JING Q, LIU R P. Preparation of the ZrTiAlV alloy with ultra-high strength and good ductility [J]. Materials Science and Engineering A, 2012, 539: 42−47.

[9] LIANG S X, YIN L X, CHE H W, JING R, ZHOU Y K, MA M Z, LIU R P. Effects of Al content on structure and mechanical properties of hot-rolled ZrTiAlV alloys [J]. Materials and Design, 2013, 52:

246−250.

[10] ZHU S, YANG H, GUO L G, FAN X G. Effect of cooling rate on microstructure evolution during α/β heat treatment of TA15 titanium alloy [J]. Materials Characterization, 2012, 70: 101−110.

[11] JING R, LIANG S X, LIU C Y, MA M Z, LIU R P. Effect of the annealing temperature on the microstructural evolution and mechanical properties of TiZrAlV alloy [J]. Materials and Design, 2013, 52: 981−986.

[12] JING R, LIANG S X, LIU C Y, MA M Z, LIU R P. Aging effects on the microstructures and mechanical properties of the Ti−20Zr−6.5Al−4V alloy [J]. Materials Science and Engineering A, 2013, 559: 474−479.

[13] LIANG S X, YIN L X, LIU X Y, JING R, ZHOU Y K, MA M Z, LIU R P. Effects of annealing treatments on microstructure and mechanical properties of the Zr345Ti35Al33V alloy [J]. Materials Science and Engineering A, 2013, 582: 374−378.

[14] QU L, YANG Z N, ZHANG F C, ZHANG M, ZHANG X Y, LIU R P. Effect of deformation and heat treatment on the microstructure and mechanical properties of β-Zr40Ti5Al4V alloy [J]. Journal of Alloys and Compounds, 2014, 612(5): 80−89.

[15] DU Z X, XIAO S L, SHEN Y P, LIU J S, LIU J, XU L J, KONG F T, CHEN Y Y. Effect of hot rolling and heat treatment on microstructure and tensile properties of high strength beta titanium alloy sheets [J]. Materials Science and Engineering A, 2015, 631: 67−74.

[16] YANG H S, GUREWITZ G, MUKHERJEE A K. Mechanical behavior and microstructural evolution during superplastic deformation of Ti−6Al−4V [J]. Materials Transactions, JIM, 1991, 32(5): 465−472.

[17] KOIKE J, SHIMOYAMA Y, OHNUMA I, OKAMURA T, KAINUMA R, ISHIDA K, MARUYAMA K. Stress-induced phase transformation during superplastic deformation in two-phase Ti−Al−Fe alloy [J]. Acta Materialia, 2000, 48(9): 2059−2069.

[18] SESHACHARYULU T, DUTTA B. Influence of prior deformation rate on the mechanism of $\beta\rightarrow\alpha+\beta$ transformation in Ti−6Al−4V [J]. Scripta Materialia, 2002, 46(9): 673−678.

[19] YU W X, LI M Q, LUO J. Effect of deformation parameters on the precipitation mechanism of secondary α phase under high temperature isothermal compression of Ti−6Al−4V alloy [J]. Materials Science and Engineering A, 2010, 527: 4210−4217.

[20] DEHGHAN-MANSHADI A, DIPPENAAR R J. Strain-induced phase transformation during thermo-mechanical processing of titanium alloys [J]. Materials Science and Engineering A, 2012, 552: 451−456.

[21] FAN X G, YANG H, GAO P F, ZUO R, LEI P H, JI Z. Morphology transformation of primary strip α phase in hot working of two-phase titanium alloy [J]. Transactions of Nonferrous Metals Society of China, 2017, 27: 1294−1305.

[22] WANG K, LI M Q. Effect of hot deformation and heat treatment on secondary α phase evolution of TC8 titanium alloy [J]. Materials Science and Engineering A, 2014, 613: 209−216.

[23] TAN Y B, LIU W C, YUAN H. LIU R P, ZHANG X Y. Hot deformation behavior of ZrTiAlV alloy with a coarse grain structure in the β phase field [J]. Materials Science and Engineering A, 2013, 577: 218−224.

[24] LUO J, LI L, LI M Q. Deformation behavior of Ti−5Al−2Sn−2Zr−4Mo−4Cr alloy with two initial microstructures during hot working [J]. Transactions of Nonferrous Metals Society of China, 2016, 26: 414−422.

[25] SESHACHARYULU T, MEDEIROS S C, FRAZIER W G, PRASAD Y V R K. Hot working of commercial Ti−6Al−4V with an equiaxed $\alpha-\beta$ microstructure: Materials modeling considerations [J]. Materials Science and Engineering A, 2000, 284: 184−194.

[26] SESHACHARYULU T, MEDEIROS S C, FRAZIER W G, PRASAD Y V R K. Microstructural mechanisms during hot working of commercial grade Ti−6Al−4V with lamellar starting structure [J]. Materials Science and Engineering A, 2002, 325(1): 112−125.

[27] TAN, Y B, JI L Y, DUAN J L, LIU W C, ZHANG J W, LIU R P. A study on the hot deformation behavior of 47Zr−45Ti−5Al−3V alloy with initial lamellar α structure [J]. Metallurgical and Materials Transactions A, 2016, 12(47): 5974−5984.

[28] TAN Y B, LIU W C, YUAN H. LIU R P, ZHANG X Y. On the phenomenon of stress drop during hot deformation of ZrTiAlV alloy [J]. Metallurgical and Materials Transactions A, 2013, 44(12): 5284−5288.

[29] DE A K, MURDOCK D C, MATAYA M C, SPEER J G, MATLOCK D K. Quantitative measurement of deformation-induced martensite in 304 stainless steel by X-ray diffraction [J]. Scripta Materialia, 2004, 50(12): 1445−1449.

[30] DONG X J, LU S Q, ZHENG H Z. Dynamic spheroidization kinetics behavior of Ti−6.5Al−2Zr−1Mo−1V alloy with lamellar microstructure [J]. Transactions of Nonferrous Metals Society of China, 2016, 26: 1301−1309.

[31] YANG G J, ZHANG T. Phase transformation and mechanical properties of the Ti50Zr30Nb10Ta10 alloy with low modulus and biocompatible [J]. Journal of Alloys and Compounds, 2005, 392(1−2): 291−294.

[32] CHEN X Z, HUANG Y M. Hot deformation behavior of HSLA steel Q690 and phase transformation during compression [J]. Journal of Alloys and Compounds, 2015, 619: 564−571.

[33] BANERJEE S. MUKHOPADHYAY P. Phase transformations: Examples from titanium and zirconium alloys [M]. Amsterdam: Elsevier, 2007: 557−584.

[34] BURKE J E. Transaction of the american institute of mining [J]. Metallurgical and Petroleum Engineers, 1949: 73−91.

[35] ZHAO Y Q, CHEN Y N, ZHANG X M, ZENG W D, WANG L. Phase transformation and heat treatment of titanium alloys [M]. Changsha: Central South University Press, 2012: 112−139. (in Chinese)

[36] FACCHINI L, MOLINARI A, HOGES S, WISSENBACH K. Ductility of a Ti−6Al−4V alloy produced by selective laser melting of prealloyed powders [J]. Rapid Prototyping Journal, 2010, 16(6): 450−459.

[37] NALLA R K, BOYCE B L, CAMPBELL J P, PETERS J O, RITCHIE R O. Influence of microstructure on high-cycle fatigue of Ti−6Al−4V: Bimodal vs lamellar structures [J]. Metallurgical and Materials Transactions A, 2002, 33(13): 899−918.

热变形对 47Zr−45Ti−5Al−3V 合金在变形过程中 $\alpha\rightarrow\beta$ 相转变的影响

谭元标[1,2]，籍丽媛[2]，刘文昌[2]，向 嵩[1]，赵 飞[1]，梁益龙[1]

1. 贵州大学 材料与冶金学院，贵州省材料结构与强度重点实验室，贵州 550025；
2. 燕山大学 材料科学与工程学院，亚稳材料制备技术与科学国家重点实验室，秦皇岛 066004

摘 要：研究应变速率和变形温度对具有初始片状 α 相的 47Zr−45Ti−5Al−3V 合金在热变形过程 $\alpha\rightarrow\beta$ 相转变的影响。结果表明，当变形温度为 550 ℃ 时，α 相的体积分数随应变速率的增加而降低；而当变形温度为 600 和 650 ℃ 时，随应变速率从 1×10^{-3} s^{-1} 增大到 1×10^{-2} s^{-1}，α 相的体积分数先增加到一个最大值，随后随应变速率的增加而逐渐下降；当变形温度为 700 ℃ 时，整个变形过程中合金组织由单一 β 相组成。在一个给定的应变速率条件下，α 相的体积分数随着变形温度的增加而降低。随着应变速率的降低和变形温度的增加，球状 α 相的体积分数和尺寸逐渐增加。当变形温度达到 650 ℃ 和应变速率降低到 1×10^{-3} s^{-1} 时，片状 α 相完全转变为球状 α 相。α 相的体积分数及形貌随应变速率和变形温度的变化显著影响合金的硬度。

关键词：47Zr−45Ti−5Al−3V 合金；热变形；相转变；维氏硬度；显微组织

(Edited by Wei-ping CHEN)